

Continual 3D Convolutional Neural Networks for Real-time Processing of Videos

Lukas Hedegaard

Alexandros Iosifidis

Department of Electrical and Computer Engineering, Aarhus University, Denmark

{lhm, ai}@ece.au.dk

Abstract

This paper introduces *Continual 3D Convolutional Neural Networks (Co3D CNNs)*, a new computational formulation of spatio-temporal 3D CNNs, in which videos are processed frame-by-frame rather than by clip. In online processing tasks demanding frame-wise predictions, Co3D CNNs dispense with the computational redundancies of regular 3D CNNs, namely the repeated convolutions over frames, which appear in multiple clips. While yielding an order of magnitude in computational savings, Co3D CNNs have memory requirements comparable with that of corresponding regular 3D CNNs and are less affected by changes in the size of the temporal receptive field. We show that Continual 3D CNNs initialised on the weights from pre-existing state-of-the-art video recognition models reduce the floating point operations for frame-wise computations by 10.0–12.4 \times while improving accuracy on Kinetics-400 by 2.3–3.8%. Moreover, we investigate the transient start-up response of Co3D CNNs and perform an extensive benchmark of online processing speed as well as accuracy for publicly available state-of-the-art 3D CNNs on modern hardware.

1. Introduction

Through the availability of large-scale open-source datasets such as ImageNet [30] and Kinetics [21, 2], deep, over-parameterized Convolutional Neural Networks (CNNs) have achieved impressive results in the field of computer vision. In video recognition specifically, 3D CNNs have lead the recent state-of-the-art [3, 36, 8, 7], generally outperforming RNN-based approaches [5, 17]. Despite their success in competitions and benchmarks where only prediction quality is evaluated, their computational cost and processing time remains a challenge to the deployment in many real-life use-cases with energy constraints and/or real-time needs. To combat this general issue, multiple approaches have been explored. These include com-

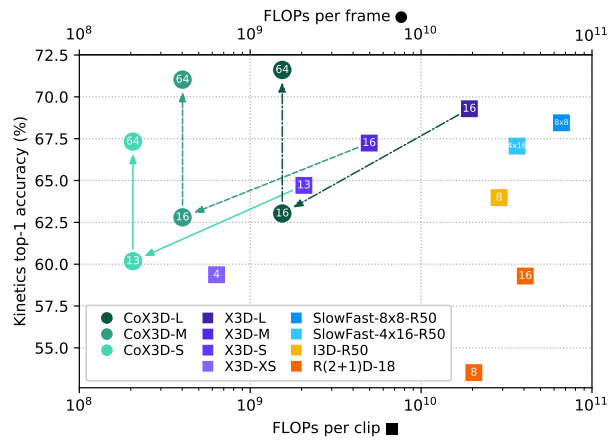


Figure 1: **Accuracy/complexity trade-off** for Continual X3D (CoX3D) and recent state-of-the-art 3D CNNs on Kinetics-400 using 1-clip/frame testing. For regular 3D CNNs, the FLOPs per clip \blacksquare are noted, while the FLOPs per frame \bullet are shown for the Continual 3D CNNs. The CoX3D models used the weights from the X3D models without further fine-tuning. The global average pool size for the network is noted in each point. The diagonal and vertical arrows indicate respectively a transfer from regular to Continual 3D CNN and an extension of receptive field.

putationally efficient architectures for image [13, 42, 34] and video recognition [24, 7, 43], pruning of network weights [4, 10, 11], knowledge distillation [12, 41, 29], and network quantisation [15, 1, 9].

The contribution in this paper is complementary to all of the above. It exploits the computational redundancies in the application of regular spatio-temporal 3D CNNs to a continual video stream in a sliding window fashion (Fig. 2). This redundancy was also explored recently [22, 31] using specialised architectures. However, these are not weight-compatible with regular 3D CNNs. In this work, we present a weight-compatible reformulation of the 3D CNN and its components as a *Continual 3D Convolutional Neural*

Network (*Co3D CNN*). *Co3D CNNs* process input videos frame-by-frame rather than clip-wise and can reuse the weights of regular 3D CNNs, producing identical outputs for networks without temporal zero-padding. To explore the characteristics of Continual CNNs and validate their efficacy, we perform conversions from three state-of-the-art 3D CNNs, each at different points on the accuracy/speed pareto-frontier, and evaluate their frame-wise performance. While there is a slight reduction in accuracy in the conversion due to zero-padding in the regular 3D CNNs, a simple network modification of extending the temporal receptive field recovers and improves the accuracy significantly *without* any fine-tuning at a negligible increase in computational cost. Furthermore, we measure the transient network response at start-up, and perform extensive benchmarking on common hardware and embedded devices to gauge the expected inference speeds for real-life scenarios. We find that Continual 3D CNNs offer a $10.0\text{--}12.4\times$ reduction in floating point operations (FLOPs), a $5.9\text{--}9.2\times$ speed increase on CPU and a $2.8\text{--}3.8\%$ accuracy improvement on Kinetics-400 over regular 3D CNNs.

2. Related Works

2.1. 3D CNNs for video recognition

Convolutional Neural Networks with spatio-temporal 3D kernels may be considered the natural extension from 2D CNNs for image recognition to CNNs for video recognition. Although they did not surpass their 2D CNN + RNN competitors [5, 17] initially [16, 20, 35], arguably due to a high parameter count and insufficient dataset size, 3D CNNs have produced state-of-the-art results [3, 36, 8] since the Kinetics dataset [21] was introduced. Yet, high accuracy comes with a high computational cost, which is prohibitive to many real-life use cases.

In image recognition, efficient architectures such as MobileNet [13], ShuffleNet [42], and EfficientNet [34] attained improved accuracy-complexity trade-offs. These architectures were extended to 3D-convolutional versions 3D-MobileNet [24], 3D-ShuffleNet [24] and X3D [7] (\approx 3D-EfficientNet) with similarly improved pareto-frontier in video-recognition tasks. While these efficient 3D CNNs work well for offline processing of videos, they are limited in the context of online processing, where we wish to make multiple predictions per second; real-time processing rates can still be achieved only at the price of severely reduced accuracy. At the heart of the limitation of 3D CNNs is the restriction that they must process a whole “clip” (spatio-temporal volume) at a time. When predictions are needed for each frame, this imposes a significant overhead due to repeated computations. In our work, we overcome this challenge by introducing an alternative computational scheme for spatio-temporal convolutions, -pooling, and -residuals,

which lets us compute 3D CNN outputs frame-wise (continually) and dispose of the redundancies produced by regular 3D CNNs.

2.2. Architectures for online video recognition

In vision tasks with a temporal dimension, a straightforward and well-explored approach [5, 17, 18, 32] is to let each frame pass through a 2D CNN trained on ImageNet in one stream alongside a second stream of Optical Flow [6]. The outputs can then be integrated using a recurrent network to model long-term temporal dependencies [5, 17] or used for spatio-temporal action detection tasks [18, 32]. It has the advantage that it requires no network modification for deployment in online-processing scenarios, lends itself to caching [40], and is free of the computational redundancies experienced in 3D CNNs. It has the disadvantage that the inclusion of optical flow introduces a large computational overhead.

Another approach is to utilise 3D CNNs for spatio-temporal feature extraction. In [27], spatio-temporal features from non-overlapping clips are used to train a recurrent network for hand gesture recognition. In [23], a 3D CNN operating on a sliding window of the input performs spatio-temporal action detection. These 3D CNN-based methods have the disadvantage of either not producing predictions for each input frame [27] or suffering from redundant computations from overlapping input clips [23].

Exploring modifications of the spatio-temporal 3D convolution operating frame by frame, the Recurrent Convolutional Unit (RCU) [31] replaces the 3D convolution by aggregating a spatial 2D convolution over the current input with a 1D convolution over the prior output. Closest to our work are Dissected 3D CNNs [22] (D3D). They define an architecture that caches the $1 \times n_H \times n_W$ frame-level features of network residual connections and concatenates them with the corresponding features in the next frame. This produces intermediary spatio-temporal features of shape $2 \times n_H \times n_W$, which become inputs to a block of convolutional layers. With kernel sizes $k_T \times k_H \times k_W$ of $2 \times 3 \times 3$ and $1 \times 3 \times 3$, the block produces features of shape $1 \times n_H \times n_W$ to be cached once again. Here, n denotes the feature map size and k the kernel size and subscripts T , H , and W denote the time, height, and width dimensions. An LSTM is then used for late spatio-temporal modelling prior to prediction. Like the Continual Convolutions that we propose, both RCU and D3D are causal and operate frame-by-frame. However, they are incompatible with pre-trained 3D CNNs, and must be trained from scratch. While the idea of caching features is also central to our work, we reformulate spatio-temporal 3D convolutions in a one-to-one compatible manner, allowing us to reuse existing model weights. In fact, all of the results presented in this paper were achieved without any training!

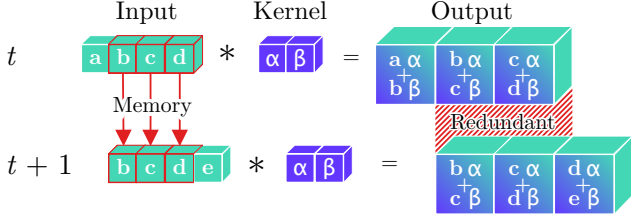


Figure 2: **Redundant computations** for a temporal convolutional layer during online processing of video clips, as illustrated by the repeated convolution of inputs (green b, c, d) with a kernel (blue α, β) in the temporal dimension. Moreover, prior inputs (b, c, d) must be stored between time-steps for online processing tasks.

3. Continual Convolutional Neural Networks

3.1. Regular 3D-convolutions lead to redundancy

Currently, the best performing architectures (X3D [7], SlowFast [8], etc.) employ variations on 3D convolutions as their main building block and perform predictions for a spatio-temporal input volume (video-clip). These architectures achieve high accuracy with reasonable computational cost for predictions on clips in the offline setting. They are, however, ill-suited for online video classification, where the input is a continual stream of video frames and a class prediction is needed for each frame. For regular 3D CNNs processing clips of m_T frames to be used in this context, prior $m_T - 1$ input frames need to be stored between temporal time-steps and assembled to form a new video-clip when the next frame is sampled. This is illustrated in Fig. 2.

Recall the computational complexity for a 3D convolution:

$$\mathcal{O}([k_H \cdot k_W \cdot k_T + b] \cdot c_I \cdot c_O \cdot n_H \cdot n_W \cdot n_T), \quad (1)$$

where k denotes the kernel size, T , H , and W are time, height, and width dimension subscripts, $b \in \{0, 1\}$ indicates whether bias is used, and c_I and c_O are the number of input and output channels. The size of the output feature map is $n = (m + 2p - d \cdot (k - 1) - 1) / s + 1$ for an input of size m and a convolution with padding p , dilation d , and stride s . During online processing, every frame in the continual video-stream will be processed n_T times (once for each position in the clip), leading to a redundancy proportional with $n_T - 1$. Moreover, the memory-overhead of storing prior input frames is

$$\mathcal{O}(c_I \cdot m_H \cdot m_W \cdot [m_T - 1]), \quad (2)$$

and during inference the network has to transiently store feature-maps of size

$$\mathcal{O}(c_O \cdot n_H \cdot n_W \cdot n_T). \quad (3)$$

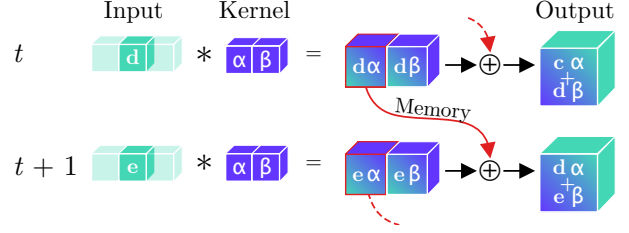


Figure 3: **Continual Convolution**. An input (green d or e) is convolved with a kernel (blue α, β). The intermediary feature-maps corresponding to all but the last temporal position are stored, while the last feature map and prior memory are summed to produce the resulting output. For a continual stream of inputs, Continual Convolutions produce identical outputs to regular convolutions.

3.2. Continual Convolutions

We can remedy the issue described in Section 3.1 by employing an alternative sequence of computational steps. In essence, we reformulate the repeated convolution of a (3D) kernel with a (3D) input-clip that continually shifts along the temporal dimension as a *Continual Convolution* (*CoConv*), where all convolution computations (bar the final sum) for the (3D) kernel with each (2D) input-frame are performed in one time-step. Intermediary results are stored as states to be used in subsequent steps, while previous and current results are summed up to produce the output. The process for a 1D input and kernel, which corresponds to the regular convolution in Fig. 2, is illustrated in Fig. 3. In general, this scheme can be applied for online-processing of any ND input, where one dimension is a temporal continual stream. Continual Convolutions are causal [37] with no information leaking from future to past and can be efficiently implemented by zero-padding the input frame along the temporal dimension with $p = \text{floor}(k/2)$. Python-style pseudo-code of the implementation is shown in Listing 1.

In terms of computational cost, we can now perform frame-by-frame computations much more efficiently than a regular 3D convolution. The complexity of processing a frame becomes:

$$\mathcal{O}([k_H \cdot k_W \cdot k_T + b] \cdot c_I \cdot c_O \cdot n_H \cdot n_W). \quad (4)$$

This reduction in computational complexity comes at the cost of a memory-overhead in each layer due to the state that is kept between time-steps. The additional overhead of storing the partially computed feature-maps for a frame is:

$$\mathcal{O}(d_T \cdot [k_T - 1] \cdot c_O \cdot n_H \cdot n_W). \quad (5)$$

However, in the context of inference in a deep neural network, the transient memory usage within each time-step is reduced by a factor of n_T to

$$\mathcal{O}(c_O \cdot n_H \cdot n_W). \quad (6)$$

```

def coconv3d(frame, prev_state = (mem, i)):
    frame = spatial_padding(frame)
    frame = temporal_padding(frame)
    feat = conv3d(frame, weights)
    output, rest_feat = feat[0], feat[1:]

    mem, i = prev_state or init_state(output)
    M = len(mem)

    for m in range(M):
        output += mem[(i + m) % M, M - m - 1]
    output += bias

    mem[i] = rest_feat
    i = (i + 1) % M

    return output, (mem, i)

```

Listing 1: **Pseudo-code** for Continual Convolution. The full implementation is available at <https://github.com/lukashedegaard/co3d>.

The benefits of Continual Convolutions thus include the independence of clip length on the computational complexity, state overhead, and transient memory consumption. The change from (non-causal) regular convolutions to (causal) Continual Convolutions has the side-effect of introducing a delay to the output. This is because some intermediary results of convolving a frame with the kernel are only added up at a later point in time (see Fig. 3). The delay for a continual convolution is

$$\mathcal{O}(d_T \cdot [k_T - 1]). \quad (7)$$

3.3. Continual Residuals

The delay from Continual Convolutions has an adverse side-effect on residual connections. Despite their simplicity in regular CNNs, we cannot simply add the input to a Continual Convolution with its output because the *CoConv* may delay the output. Residual connections to a *CoConv* must therefore be delayed by an equivalent amount (see Eq. (7)). This produces a memory overhead of

$$\mathcal{O}(d_T \cdot [k_T - 1] \cdot c_O \cdot m_H \cdot m_W). \quad (8)$$

3.4. Continual Pooling

The associative property of pooling operations allows for pooling to be decomposed across dimensions, i.e. $\text{pool}_{T,H,W}(\mathbf{X}) = \text{pool}_T(\text{pool}_{H,W}(\mathbf{X}))$. For continual spatio-temporal pooling, the pooling over spatial dimensions is equivalent to a regular pooling, while the intermediary pooling results must be stored for prior temporal frames. For a pooling with temporal kernel size k_T and spatial output size $n_H \cdot n_W$, the memory consumption is

$$\mathcal{O}([k_T - 1] \cdot n_H \cdot n_W), \quad (9)$$

and the delay is

$$\mathcal{O}(k_T - 1). \quad (10)$$

Both memory consumption and delay scale linearly with the temporal kernel size. Fortunately, the memory consumed by temporal pooling layers is relatively modest for most CNN architectures (1.5% for *CoX3D-M*, see Appendix A). Hence, the delay rather than memory consumption may be of primary concern for real-life applications. For some network modules it may even make sense to skip the pooling in the conversion to a Continual CNN. One such example is the 3D Squeeze-and-Excitation (SE) block [14] in X3D, where global spatio-temporal average-pooling is used in the computation of channel-wise self-attention. Discarding the temporal pooling component (making it a 2D SE block) shifts the attention slightly (assuming the frame contents change slowly relative to the sampling rate) but avoids a considerable temporal delay.

3.5. The issue with temporal padding

Zero-padding of convolutional layers is a popular strategy for retaining the spatio-temporal dimension of a feature-map between consecutive layers in a CNN. For Continual CNNs, however, temporal zero-padding poses a problem, as illustrated in Fig. 4. Consider a 2-layer 1D CNN where each layer has a kernel size of 3 and zero padding of 1. For each new frame in a continual stream of inputs, the first layer l should produce two output feature-maps: One by the convolution of the two prior frames and the new frame, and another by convolving with one prior frame, the new frame, and a zero-pad. The next layer $l + 1$ thus receives two inputs and produces three outputs which are dependent on the new input frame of the first layer (one for each input and another from zero-padding). In effect, each zero padding in a convolution forces the next layer to retrospectively update its output for a previous time-step in a non-causal manner. As we move through layers, the available computational redundancy to be exploited by Continual Convolutions is gradually reduced. Thus, there is a considerable downside to the use of padding.

This questions the necessity of zero padding along the temporal dimension. In regular CNNs, zero padding has two benefits: It helps to avoid spatio-temporal shrinkage of feature-maps when propagated through a deep CNN, and it prevents information at the borders from “washing away” [19]. The use of zero-padding, however, has the downside that it alters the input-distribution along the borders significantly [25, 28]. For input data which is a continual stream of frames, a shrinkage of the feature-size in the temporal dimension is not a concern, and an input frame (which may be considered a border frame in regular 3D CNN) has no risk of “washing away” because it is a middle frame in subsequent time steps. Temporal padding is thus omitted in Continual CNNs. As can be seen in the experimental evaluations presented in the following, this constitutes an approximation error in the conversion from reg-

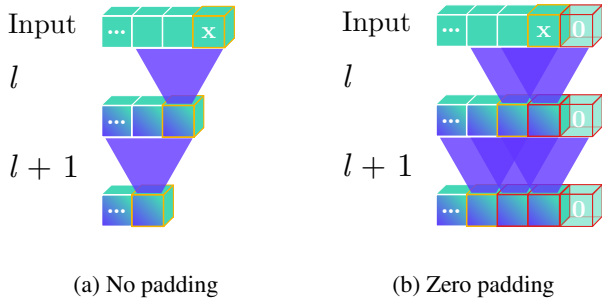


Figure 4: **Issue with temporal padding:** The latest frame \mathbf{x} is propagated through a CNN with (purple) temporal kernels of size 3 (a) without or (b) with zero padding. Highlighted cubes can be produced only in the latest frame, with yellow boarder indicating independence of padded zero and red boarders dependence. In the zero-padded case (b), the number of frame features dependent on \mathbf{x} following a layer l increases with the number of padded zeros.

ular to Continual 3D CNN if the former was trained with temporal padding.

3.6. Initialisation

Before a Continual CNN reaches a steady state of operation, it must have processed $r_T - 1$ frames where r_T is the receptive field size of the network in the temporal dimension. For example, the Continual X3D- $\{S, M, L\}$ models have receptive fields of size $\{69, 72, 130\}$. There is thus a transient network response at start-up. This response depends on how internal state variables are initialised. Here, we propose two variants: 1) Initialisation with *zeros* and 2) by repeating a *replicate* of the features corresponding to the first input-frame. The latter corresponds to operating in a steady state for a “boring video” [3] which has one frame repeated in the entire clip.

3.7. Memory consumption: A case study

Where does this leave us with regards to the memory consumption during inference in online-scenarios? To gauge this, we can compare the worst-case memory consumption for the regular X3D-M model [7] with the corresponding Continual X3D-M (*CoX3D-M*) model. Disregarding the storage requirement of the model weights (which is identical for both regular and continual model versions), the memory consumption of storing input-frames between time-steps for the regular model is computed by Eq. (2): For a clip size of $m_T \times m_H \times m_W = 16 \times 224 \times 224$, the memory requirement is $3 \cdot (16 - 1) \cdot 224 \cdot 224 = 2,257,920$ floating point numbers (floats). The final consumption in bytes depends on the floating-point precision. In addition, we need to account for the transient memory consumption,

which occurs while storing the intermediary feature-maps. The worst case is the output of the first convolution which is of size $24 \times 16 \times 112 \times 112$ corresponding to 4,816,896 floats. Thus, the regular X3D-M has a worst-case total memory-consumption of 7,074,816 floats.

The continual version of X3D-M (*CoX3D-M*) has no need to store input frames between time-steps, but it must keep state for the Continual Convolutions, Continual Pooling and Continual Residuals. 6,107,568 floats are stored as state within the *CoX3D-M* model (see Appendix A). The worst-case transient memory again occurs while storing the first feature-map, but this time it is only of size $24 \times 1 \times 112 \times 112$, or 301,056 floats. The Continual X3D-M thus has a worst case total memory-consumption of 6,408,624 floats. This corresponds to a 9.4% reduction in total memory-requirements relative to the regular model.

3.8. Design considerations

It should be noted that the result of the comparison in Section 3.7 is highly dependent on the clip size used by the regular model. For a clip size of 4 frames (as in X3D-XS), X3D-M₄ would have a worst-case memory consumption of 1,655,808 floats. Its continual counterpart, in which the temporal kernel size of the final pooling layer is reduced to 4, needs 6,403,440 floats. Thus, it may still be worth considering the use of the regular CNN in some embedded systems, which are severely constrained on memory, if lowering the spatial resolution is not an option. On the other hand, using a larger clip size of 64, X3D-M₆₄ would consume 28,449,792 floats, whereas *CoX3D-M*₆₄ has a worst-case consumption of only 6,429,360 floats. This simple example demonstrates that Continual CNNs utilise longer effective clip sizes much more efficiently than regular CNNs in on-line processing scenarios. In networks intended for embedded systems or online processing scenarios, we may thus increase the clip size to achieve higher accuracy with minimal penalty in computational complexity and worst-case memory consumption.

Another design-consideration, which has a considerable influence on memory consumption is the temporal kernel size and dilation of *CoConv* layers. Fortunately, the trend to employ small kernel sizes leaves the memory consumption reasonable for current state-of-the-art networks [3, 36, 8, 7]. A larger temporal kernel size would not only affect the memory growth through the *CoConv* filter, but also for co-occurring residual connections, since these consume a significant fraction of the total state-memory for real-life networks; in a Continual X3D-M model (*CoX3D-M*) the memory of residual constitutes 31.6% of the total model state memory (see Appendix A).

Model	Acc. (%)	Params (M)	FLOPs (G)	Speed (evaluations/s)				
				CPU	TX2	Xavier	RTX 2080 Ti	
I3D-R50	63.98	28.04	28.61	0.93 ± 0.04	2.54 ± 0.02	5.37 ± 0.01	77.15 ± 0.88	
R(2+1)D-18 ₈	53.52	31.51	20.35	1.75 ± 0.11	3.19 ± 0.04	6.82 ± 0.01	130.88 ± 0.29	
R(2+1)D-18 ₁₆	59.29	31.51	40.71	0.83 ± 0.06	1.82 ± 0.01	3.77 ± 0.01	75.81 ± 0.21	
SlowFast-8×8-R50	68.45	66.25	50.72	0.34 ± 0.01	0.87 ± 0.00	1.66 ± 0.03	30.72 ± 0.34	
SlowFast-4×16-R50	67.06	34.48	36.46	0.55 ± 0.02	1.33 ± 0.01	2.13 ± 0.05	41.28 ± 0.51	
X3D-L	69.29	6.15	19.17	0.25 ± 0.01	0.19 ± 0.00	0.88 ± 0.00	16.58 ± 0.13	
X3D-M	67.24	3.79	4.97	0.83 ± 0.04	1.47 ± 0.00	3.69 ± 0.02	55.27 ± 0.67	
X3D-S	64.71	3.79	2.06	2.23 ± 0.11	2.68 ± 0.01	8.07 ± 0.12	138.04 ± 1.69	
X3D-XS	59.37	3.79	0.64	8.26 ± 0.11	8.20 ± 0.09	26.37 ± 0.03	430.15 ± 9.29	
Frame	CoX3D-L ₁₆	63.03	6.15	1.54	2.30 ± 0.07	0.99 ± 0.00	6.30 ± 0.00	101.38 ± 3.36
	CoX3D-L ₆₄	71.61	6.15	1.54	2.30 ± 0.08	0.99 ± 0.00	6.30 ± 0.01	111.53 ± 4.55
	CoX3D-M ₁₆	62.80	3.79	0.40	7.57 ± 0.14	7.26 ± 0.13	23.70 ± 0.09	335.42 ± 9.91
	CoX3D-M ₆₄	71.03	3.79	0.40	7.51 ± 0.17	7.04 ± 0.03	23.70 ± 0.09	323.56 ± 9.91
	CoX3D-S ₁₃	60.18	3.79	0.21	13.16 ± 0.35	11.06 ± 0.03	40.09 ± 0.04	722.43 ± 56.95
	CoX3D-S ₆₄	67.33	3.79	0.21	13.19 ± 0.37	11.13 ± 0.04	40.10 ± 0.04	726.81 ± 67.38

Table 1: **Benchmark of state-of-the-art methods on Kinetics-400.** The noted accuracy is the single clip or frame top-1 score using RGB as the only input-modality. The performance was evaluated using publicly available pre-trained models without any further fine-tuning. For speed comparison, evaluations per second denote frames per second for the *CoX3D* models and clips per second for the remaining models. Speed results are the mean \pm std of 100 measurements.

4. Experiments

The experiments in this section aim to show the characteristics and advantages of Continual 3D CNNs as compared with regular 3D CNNs. One of the main benefits of *Co3D* CNNs is their ability to reuse the network weights of regular 3D CNNs. As such, all *Co3D* CNNs in these experiments use network weights that were pre-trained with Kinetics-400 [21] on regular 3D CNNs without further fine-tuning. Unless stated otherwise, we use the data same pre-processing steps as [8, 7].

The section is laid out as follows: First, we showcase the network performance following weight transfer from regular to Continual 3D. This is followed by a study on the transient response of *Co3D* CNNs at startup. Furthermore, we show how the computational advantages of *Co3D* CNNs can be exploited to improve accuracy by extending the temporal receptive field. Finally, we perform an extensive benchmark of prior state-of-the-art methods and Continual 3D CNNs, measuring the 1-clip/frame accuracy of publicly available models, as well as their inference speed on various computational devices.

4.1. Transfer from regular to Continual CNNs

There is a one-to-one correspondence between the weights in a regular CNN and the continual version of the same network. Because Continual CNNs do not utilise zero-padding, however, there is a computational discrepancy between them. To gauge the direct transferability of knowledge to Continual CNNs, we initialise a set of

Continual X3D (*CoX3D*) networks with Kinetics-400 pre-trained X3D network weights [7]. The publicly available X3D network variants XS, S, M, and L were evaluated on the Kinetics-400 test set using one temporally centred clip from each video. We omit the XS network in the transfer to *CoX3D*, given that it is architecturally equivalent to S, but with fewer frames per clip. In evaluation of the continual networks, we faced the challenge that the Kinetics videos were all limited to 10 seconds. Due to the relatively long transient response of Continual CNNs (see Section 4.2) and low frame-rate used for training the X3D models (5.0, 6.0, 6.0 FPS for S, M, and L respectively), the video-length was insufficient to reach steady-state. As a practical measure to evaluate near steady-state, we repeated the last video-frame for a padded video length of $\approx 80\%$ of the network receptive field as a heuristic choice. The Continual CNNs were thus tested on the last frame of the padded video and initialised with the prior frames.

The results of the transfer are shown in Table 1 and Fig. 1. For all networks, the transfer from regular to Continual 3D CNN results in significant computational savings. For the S, M, and L networks the reduction in FLOPs is $10.0\times$, $12.4\times$, and $12.4\times$ respectively. These savings are less than the clip size due to the final pooling and prediction layers, which are in use for each frame in the Continual CNN, but only once per clip in regular CNNs. As a side-effect of the transfer from zero-padded regular CNN to Continual CNN without zero-padding, we see a noticeable reduction in accuracy. This reduction is easily improved by

using an extended pooling size for the network (discussed in Section 3.8 and in Section 4.3). Using a global average pooling with temporal kernel size 64, we improve the accuracy of X3D by 2.6%, 3.8%, and 2.3% in the Continual S, M, and L network variants. As noted earlier, the Kinetics dataset did not have sufficient frames to fill the temporal receptive field of the Continual CNNs in these tests. The results in Table 1 are thus lower than what may be expected for online scenarios given enough frames. We explore this further in Sections 4.2 and 4.3.

4.2. Transient response of Continual CNNs

As described in Section 3.6, Continual CNNs exhibit a transient response during their up-start. In order to gauge this response, we perform a set of experiments on the Kinetics-400 validation set, this time sampled at 15 FPS to have a sufficient number of frames available. This corresponds to a data domain shift [38] relative to the pre-trained weights, where time advances slower. First, we check the baseline X3D network 1-clip accuracy, which will constitute the expected upper bound. Then we evaluate the *CoX3D* frame accuracy with X3D weights, varying the number of prior frames used for initialisation. Note that temporal center-crops of size $T_{init} + 1$, where T_{init} is the number of initialisation frames, are used in each evaluation to ensure that the frames seen by the network come from the centre. This precaution is used to counter a data-bias, we noticed in Kinetics-400, namely that the start and end of a video are less informative and contribute to worse predictions than the central part. For an X3D-S network evaluated at different video positions, the results can vary up to 8%. The experiment is repeated for two initialisation schemes, “zeros” and “replicate”, and two model sizes, S and M. The measured transient responses are shown in Fig. 5.

For all responses, the first ≈ 25 frames produce near-random predictions, before rapidly increasing at 25–30 frames until a steady-state is reached at 49.2% and 56.2% accuracy for S and M. Relative to the regular X3D, this constitutes a steady-state error of -1.7% and -5.8% . Comparing initialisation schemes, we see that the “replicate” scheme results in a slightly earlier rise. The rise sets in later for the “zeros” scheme, but exhibits a sharper slope, overshooting the steady-state accuracy (with peaks at 51.6% and 57.6%) before settling at the exact same values as for the “replication” scheme. This overshoot response was unexpected, and our best conjecture is that the network benefits from some zero states because the regular network, from which is inherited its parameters, was trained using zero padding. While this overshoot could be exploited to inflate the measured accuracy, we abstain from this practice and report only accuracy for steady-state or the latest-possible frame while using “replicate” padding in case of insufficient frames in the video.

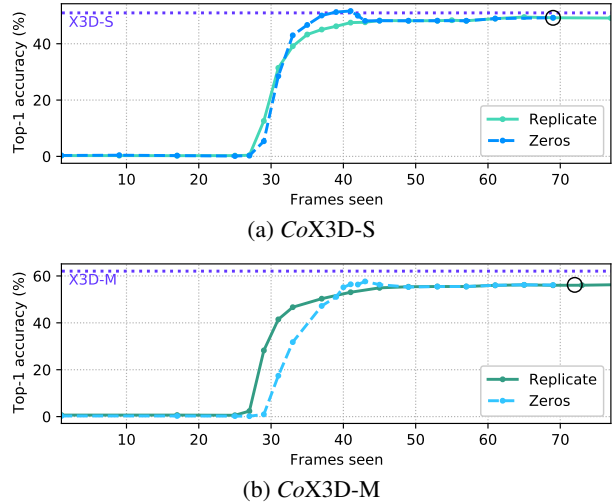


Figure 5: **Transient response** for Continual X3D- $\{S,M\}$ on the Kinetics-400 validation set at 15 FPS. The dotted horizontal lines constitute the X3D validation accuracy for 1-clip predictions. The black circles highlight when the frames seen equal the receptive field of the networks.

4.3. Extended receptive field

Continual CNNs experience a negligible increase in computational cost when larger temporal receptive field are used (see Section 3.8). For *CoX3D* networks, this extension can be trivially implemented by increasing the temporal kernel size of the last pooling layer. In this set of experiments, we extend *CoX3D*- $\{S,M,L\}$ to have temporal pooling sizes 32, 64, and 96, and evaluate them on the Kinetics-400 validation set sampled at 15 FPS. Note, once again, that the network weights were trained on a different sampling rate. The Continual CNNs are evaluated at frames corresponding to the steady state.

Table 2 shows the measured accuracy and floating point operations per frame (*CoX3D*) / clip (X3D) as well as the pool size for the penultimate network layer (global average pooling) and the total receptive field of the network in the temporal dimension. A corresponding visual depiction is found in Fig. 6. As found in Section 4.1, each transfer results in significant computational savings alongside a drop in accuracy. Extending the kernel size of the global average pooling layer increases the accuracy of the Continual CNNs by 11.0–13.3% for 96 frames relative to the original 13-16 frames, surpassing that of the regular CNNs. Lying at 0.017–0.009%, the corresponding computational increases can be considered negligible.

4.4. Inference benchmarks

Despite their high status in activity recognition leaderboards [39], it is unclear how the state-of-the-art methods of late perform in the online setting, where speed and ac-

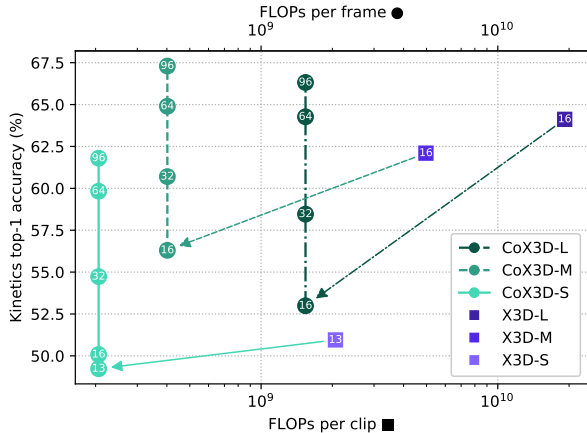


Figure 6: **Accuracy versus FLOPs for extended receptive fields** on the Kinetics-400 validation set at 15 FPS. The global average pool size along the temporal dimension is indicated in each point, and the arrows denote a one-to-one transfer from regular to Continual X3D without fine-tuning.

accuracy constitute a necessary trade-off. Specifically, many methods sample multiple clips from different spatial and temporal positions in a video and average the predictions to produce their best results. To avoid the high computational cost of this practice, a reasonable tactic in the online setting is to make predictions from only a single clip. The number of FLOPs as a proxy for inference speed is occasionally noted, but to the best of our knowledge, there has not yet been a systematic evaluation of inference speed for these video-recognition models on real-life hardware. In this set of experiments, we benchmark the 1-clip accuracy of I3D-R50 [3], R(2+1)D-18 [36], SlowFast-8×8-R50 and SlowFast-4×16-R50 [33], as well as the X3D model family [7] alongside the 1-frame accuracy of *CoX3D*. To gauge the achievable speeds at different computational budgets, the networks were tested on four hardware platforms as described in Appendix B.

The results of the benchmark are found in Table 1. Due to the limitation to a single clip, we see that achieved accuracy for the baselines is generally lower than published in the respective works [3, 36, 8, 7]. The speed evaluation results are approximately (inversely log-log) proportional to the measured FLOPs. They are, however skewed to the low side for X3D models, confirming the observation in [26] that FLOPs are not always an accurate proxy for the inference speed on real-life hardware due to differences in memory access cost. Across hardware platforms, the *CoX3D* models with extended receptive fields attain the best accuracy/speed trade-off by a large margin. For example, *CoX3D-S*₆₄ achieves an accuracy of 67.3% at 40.1 frames per second on the Nvidia Jetson Xavier, compared to 59.4% accuracy at 26.4 clips per second for X3D-XS.

Model	Size	Pool	Acc.	FLOPs (K)	Rec. Field
X3D	S	13	51.0	2,061,366	13
	M	16	62.1	4,970,008	16
	L	16	64.1	19,166,052	16
<i>CoX3D</i>	S	13	49.2	205,933	69
		16	50.1	205,934	72
		32	54.7	205,941	88
	M	64	59.8	205,955	120
		96	61.8	205,968	152
		16	56.3	401,829	72
	L	32	60.7	401,836	88
		64	64.9	401,850	120
		96	67.3	401,864	152
L	16	53.0	1,540,474	130	
	32	58.5	1,540,481	146	
	64	64.3	1,540,495	178	
		96	66.3	1,540,509	210

Table 2: **Effect of extending pool size.** Note that the model weights were trained at different sampling rates than evaluated at (15 FPS), resulting in a lower top-1 validation accuracy on Kinetics-400 than was originally reported in [7]. *Italic numbers* denote measurement taken within the transient response due to a lack of frames in the video-clip.

5. Conclusion

We have introduced Continual 3D Convolutional Neural Networks (*Co3D* CNNs), a new computational model for spatio-temporal 3D CNNs, which performs computations frame-wise rather than clip-wise while being weight-compatible with regular 3D CNNs. In doing so, we are able to dispose of the computational redundancies faced by 3D CNNs in continual online processing, leading to a 10.0–12.4× reduction of floating point operations, a 5.9–9.2× real-life inference speed-up, and an accuracy improvement of 2.8–3.8% on Kinetics-400 through an extension in the global average pooling kernel size.

While this constitutes a substantial leap in the processing efficiency of energy-constrained and real-time video recognition systems, there are still unanswered questions pertaining to the dynamics of *Co3D* CNNs. Specifically, the impact of extended receptive fields on the networks ability to change predictions in response to changing contents in the input video is untested. We leave this as an important direction for future work.

Acknowledgement

This work has received funding from the European Union’s Horizon 2020 research and innovation programme under grant agreement No 871449 (OpenDR). This publication reflects the authors’ views only. The European Commission is not responsible for any use that may be made of the information it contains.

References

- [1] Z. Cai, X. He, J. Sun, and N. Vasconcelos. Deep learning with low precision by half-wave gaussian quantization. In *2017 IEEE Conference on Computer Vision and Pattern Recognition (CVPR)*, pages 5406–5414, 2017.
- [2] Joao Carreira, Eric Noland, Andras Banki-Horvath, Chloe Hillier, and Andrew Zisserman. A short note about kinetics-600. *preprint, arXiv:1808.01340*, 2018.
- [3] J. Carreira and A. Zisserman. Quo vadis, action recognition? a new model and the kinetics dataset. In *IEEE Conference on Computer Vision and Pattern Recognition (CVPR)*, pages 4724–4733, 2017.
- [4] Wenlin Chen, James T. Wilson, Stephen Tyree, Kilian Q. Weinberger, and Yixin Chen. Compressing neural networks with the hashing trick. In *International Conference on Machine Learning (ICML)*, page 2285–2294, 2015.
- [5] J. Donahue, L. A. Hendricks, S. Guadarrama, M. Rohrbach, S. Venugopalan, T. Darrell, and K. Saenko. Long-term recurrent convolutional networks for visual recognition and description. In *IEEE Conference on Computer Vision and Pattern Recognition (CVPR)*, pages 2625–2634, 2015.
- [6] Gunnar Farneback. Two-frame motion estimation based on polynomial expansion. In *Image Analysis*, pages 363–370. Springer Berlin Heidelberg, 2003.
- [7] Christoph Feichtenhofer. X3D: Expanding architectures for efficient video recognition. *IEEE/CVF Conference on Computer Vision and Pattern Recognition (CVPR)*, 2020.
- [8] Christoph Feichtenhofer, Haoqi Fan, Jitendra Malik, and Kaiming He. Slowfast networks for video recognition. In *IEEE/CVF International Conference on Computer Vision (ICCV)*, October 2019.
- [9] Nikolaos Floropoulos and Anastasios Tefas. Complete vector quantization of feedforward neural networks. *Neurocomputing*, 367:55–63, 2019.
- [10] Song Han, Huizi Mao, and William J. Dally. Deep compression: Compressing deep neural network with pruning, trained quantization and huffman coding. In *International Conference on Learning Representations (ICLR)*, 2016.
- [11] Y. He, X. Zhang, and J. Sun. Channel pruning for accelerating very deep neural networks. In *2017 IEEE International Conference on Computer Vision (ICCV)*, pages 1398–1406, 2017.
- [12] Geoffrey Hinton, Oriol Vinyals, and Jeffrey Dean. Distilling the knowledge in a neural network. In *NIPS Deep Learning and Representation Learning Workshop*, 2015.
- [13] Andrew G. Howard, Menglong Zhu, Bo Chen, Dmitry Kalenichenko, Weijun Wang, Tobias Weyand, Marco Andreetto, and Hartwig Adam. Mobilenets: Efficient convolutional neural networks for mobile vision applications. *preprint, arXiv:1704.04861*, abs/1704.04861, 2017.
- [14] J. Hu, L. Shen, and G. Sun. Squeeze-and-excitation networks. In *IEEE/CVF Conference on Computer Vision and Pattern Recognition (CVPR)*, pages 7132–7141, 2018.
- [15] Itay Hubara, Matthieu Courbariaux, Daniel Soudry, Ran El-Yaniv, and Yoshua Bengio. Binarized neural networks. In D. Lee, M. Sugiyama, U. Luxburg, I. Guyon, and R. Garnett, editors, *Advances in Neural Information Processing Systems*, volume 29. Curran Associates, Inc., 2016.
- [16] S. Ji, W. Xu, M. Yang, and K. Yu. 3d convolutional neural networks for human action recognition. *IEEE Transactions on Pattern Analysis and Machine Intelligence (TPAMI)*, 35(1):221–231, 2013.
- [17] Joe Yue-Hei Ng, M. Hausknecht, S. Vijayanarasimhan, O. Vinyals, R. Monga, and G. Toderici. Beyond short snippets: Deep networks for video classification. In *IEEE Conference on Computer Vision and Pattern Recognition (CVPR)*, pages 4694–4702, 2015.
- [18] V. Kalogeiton, P. Weinzaepfel, V. Ferrari, and C. Schmid. Action tubelet detector for spatio-temporal action localization. In *2017 IEEE International Conference on Computer Vision (ICCV)*, pages 4415–4423, 2017.
- [19] Andrej Karpathy. CS231n convolutional neural networks for visual recognition. URL: <https://cs231n.github.io/convolutional-networks/>. Last visited on 2021/01/26.
- [20] A. Karpathy, G. Toderici, S. Shetty, T. Leung, R. Sukthankar, and L. Fei-Fei. Large-scale video classification with convolutional neural networks. In *IEEE Conference on Computer Vision and Pattern Recognition (CVPR)*, pages 1725–1732, 2014.
- [21] Will Kay, Joao Carreira, Karen Simonyan, Brian Zhang, Chloe Hillier, Sudheendra Vijayanarasimhan, Fabio Viola, Tim Green, Trevor Back, Paul Natsev, Mustafa Suleyman, and Andrew Zisserman. The kinetics human action video dataset. *preprint, arXiv:1705.06950*, 2017.
- [22] Okan Köpüklü, Stefan Hörmann, Fabian Herzog, Hakan Cevikalp, and Gerhard Rigoll. Dissected 3d cnns: Temporal skip connections for efficient online video processing. *arXiv preprint arXiv:2009.14639*, 2020.
- [23] Okan Köpüklü, Xiangyu Wei, and Gerhard Rigoll. You only watch once: A unified cnn architecture for real-time spatiotemporal action localization. 2019.
- [24] O. Köpüklü, N. Kose, A. Gunduz, and G. Rigoll. Resource efficient 3d convolutional neural networks. In *IEEE/CVF International Conference on Computer Vision Workshop (ICCVW)*, pages 1910–1919, 2019.
- [25] Guilin Liu, Kevin J. Shih, Ting-Chun Wang, Fitsum A. Reda, Karan Sapra, Zhiding Yu, Andrew Tao, and Bryan Catanzaro. Partial convolution based padding. pages 1–11, 2018.
- [26] Ningning Ma, Xiangyu Zhang, Hai-Tao Zheng, and Jian Sun. Shufflenet v2: Practical guidelines for efficient cnn architecture design. In *Proceedings of the European Conference on Computer Vision (ECCV)*, September 2018.
- [27] P. Molchanov, X. Yang, S. Gupta, K. Kim, S. Tyree, and J. Kautz. Online detection and classification of dynamic hand gestures with recurrent 3d convolutional neural networks. In *2016 IEEE Conference on Computer Vision and Pattern Recognition (CVPR)*, pages 4207–4215, 2016.
- [28] A. Nguyen, S. Choi, W. Kim, S. Ahn, J. Kim, and S. Lee. Distribution padding in convolutional neural networks. In *International Conference on Image Processing (ICIP)*, pages 4275–4279, 2019.

- [29] Nikolaos Passalis and Anastasios Tefas. Learning deep representations with probabilistic knowledge transfer. In *Proceedings of the European Conference on Computer Vision (ECCV)*, 2018.
- [30] Olga Russakovsky, Jia Deng, Hao Su, Jonathan Krause, Sanjeev Satheesh, Sean Ma, Zhiheng Huang, Andrej Karpathy, Aditya Khosla, Michael Bernstein, Alexander C. Berg, and Li Fei-Fei. Imagenet large scale visual recognition challenge. *International Journal of Computer Vision (ICCV)*, 115(3):211–252, 2015.
- [31] G. Singh and F. Cuzzolin. Recurrent convolutions for causal 3d cnns. In *2019 IEEE/CVF International Conference on Computer Vision Workshop (ICCVW)*, pages 1456–1465, 2019.
- [32] G. Singh, S. Saha, M. Sapienza, P. Torr, and F. Cuzzolin. Online real-time multiple spatiotemporal action localisation and prediction. In *2017 IEEE International Conference on Computer Vision (ICCV)*, pages 3657–3666, 2017.
- [33] Vladislav Sovrasov. ptflops. URL: <https://github.com/sovrasov/flops-counter.pytorch>. Last visited on 2021/03/02.
- [34] Mingxing Tan and Quoc Le. EfficientNet: Rethinking model scaling for convolutional neural networks. In *Proceedings of Machine Learning Research*, volume 97, pages 6105–6114, 2019.
- [35] Du Tran, Lubomir Bourdev, Rob Fergus, Lorenzo Torresani, and Manohar Paluri. Learning spatiotemporal features with 3d convolutional networks. In *IEEE International Conference on Computer Vision (ICCV)*, pages 4489–4497, 2015.
- [36] D. Tran, H. Wang, L. Torresani, J. Ray, Y. LeCun, and M. Paluri. A closer look at spatiotemporal convolutions for action recognition. In *IEEE/CVF Conference on Computer Vision and Pattern Recognition (CVPR)*, pages 6450–6459, 2018.
- [37] Aäron van den Oord, Sander Dieleman, Heiga Zen, Karen Simonyan, Oriol Vinyals, Alexander Graves, Nal Kalchbrenner, Andrew Senior, and Koray Kavukcuoglu. Wavenet: A generative model for raw audio. In *arXiv preprint arXiv:1609.03499*, 2016.
- [38] Mei Wang and Weihong Deng. Deep visual domain adaptation: A survey. *Neurocomputing*, 312:135–153, 2018.
- [39] Papers with Code. Kinetics-400 leaderboard. URL: <https://paperswithcode.com/sota/action-classification-on-kinetics-400>. Last visited on 2021/02/03.
- [40] M. Xu, M. Zhu, Yunxin Liu, F. Lin, and X. Liu. Deepcache: Principled cache for mobile deep vision. *International Conference on Mobile Computing and Networking*, 2018.
- [41] J. Yim, D. Joo, J. Bae, and J. Kim. A gift from knowledge distillation: Fast optimization, network minimization and transfer learning. In *2017 IEEE Conference on Computer Vision and Pattern Recognition (CVPR)*, pages 7130–7138, 2017.
- [42] X. Zhang, X. Zhou, M. Lin, and J. Sun. Shufflenet: An extremely efficient convolutional neural network for mobile devices. In *IEEE/CVF Conference on Computer Vision and Pattern Recognition (CVPR)*, pages 6848–6856, 2018.
- [43] Linchao Zhu, Laura Sevilla-Lara, Yi Yang, Matt Feiszli, and Heng Wang. Faster recurrent networks for efficient video classification. *Proceedings of the AAAI Conference on Artificial Intelligence*, 34:13098–13105, 2020.

Appendix

A. Worst-case memory for *CoX3D-M*

In this section, we provide a detailed overview of the memory consumption incurred by the internal state in a Continual X3D-M (*CoX3D-M*) model. For Continual 3D CNNs, there is no need to store input frames between time steps, though this is the case for regular 3D CNNs applied in an online processing scenario. Intermediary computations from prior frames are kept in the continual layers as state if a layer has a temporal receptive field larger than 1. A continual $k_T \times k_H \times k_W = 1 \times 3 \times 3$ convolution is equivalent to a regular convolution, while a $3 \times 1 \times 1$ is not. The same principle holds for pooling layers. As a design decision, the temporal component of the average pooling of Squeeze-and-Excitation (SE) blocks is discarded. Hence, SE blocks do not incur a memory overhead or delay. Keeping the temporal pooling of the SE block would have increased memory consumption by a modest 85.050 (+1.4%). We can compute the total state overhead using Eq. (2), Eq. (8), and Eq. (9) by adding up the state size of each applicable layer shown in Table 4. An overview of the resulting computations can be found in Table 3. The total memory overhead for the network state is 6,192,618 floating point operations. In addition to the state memory, the worst-case transient memory must be taken into account. The largest intermediary feature-map is produced after the first convolution in conv_1 and has a size of $24 \times 112 \times 112 = 301,056$ floats. The total worst-case memory consumption for *CoX3D-M* (excluding models weights) is thus **6,408,624** floats.

If we were to reduce the model clip size from 16 to 4, this would result in a memory reduction of 5,184 floats (only pool_5 is affected) for a total worst-case memory of 6,102,384 floats (-0.08%). Increasing the clip size to 64 would yield an increased state memory of 20,736 floats giving a total worst-case memory of 6,128,304 floats (+0.3%).

Stage	Layer		Mem. (floats)
conv_1	conv_T	$(5 - 1) \times 24 \times 112 \times 112 =$	1,204,224
res_2	residual_1	$(3 - 1) \times 24 \times 112 \times 112 =$	602,112
	residual_{2-3}	$[(3 - 1) \times 24 \times 56 \times 56] \times 2 =$	301,056
	conv_{1-3}	$[(3 - 1) \times 54 \times 56 \times 56] \times 3 =$	1,016,064
res_3	residual_1	$(3 - 1) \times 24 \times 56 \times 56 =$	150,528
	residual_{2-5}	$[(3 - 1) \times 48 \times 28 \times 28] \times 4 =$	301,056
	conv_{1-5}	$[(3 - 1) \times 108 \times 28 \times 28] \times 5 =$	846,720
res_4	residual_1	$(3 - 1) \times 48 \times 28 \times 28 =$	75,264
	residual_{2-11}	$[(3 - 1) \times 96 \times 14 \times 14] \times 10 =$	376,320
	conv_{1-11}	$[(3 - 1) \times 216 \times 14 \times 14] \times 11 =$	931,392
res_5	residual_1	$(3 - 1) \times 96 \times 14 \times 14 =$	37,632
	residual_{2-3}	$[(3 - 1) \times 192 \times 7 \times 7] \times 6 =$	112,896
	conv_{1-3}	$[(3 - 1) \times 432 \times 7 \times 7] \times 7 =$	296,352
pool_5	-	$(16 - 1) \times 432 =$	6,480
Total			6,107,568

Table 3: *CoX3D-M* state memory consumption by layer.

Stage		Filters	Output size ($T \times H \times W$)
input		-	$16 \times 224 \times 224$
conv_1		$1 \times 3^2, 24$	$16 \times 112 \times 112$
		$5^* \times 1^2, 24$	
res_2	res	$1 \times 1^2, 54$	$\times 3$
		$3 \times 3^2, 54$	
		SE	
		$1 \times 1^2, 24$	
res_3	res	$1 \times 1^2, 108$	$\times 5$
		$3 \times 3^2, 108$	
		SE	
		$1 \times 1^2, 48$	
res_4	res	$1 \times 1^2, 216$	$\times 11$
		$3 \times 3^2, 216$	
		SE	
		$1 \times 1^2, 96$	
res_5	res	$1 \times 1^2, 432$	$\times 7$
		$3 \times 3^2, 432$	
		SE	
		$1 \times 1^2, 192$	
conv_5		$1 \times 1^2, 432$	$16 \times 7 \times 7$
pool_5		16×7^2	$1 \times 1 \times 1$
fc_1		$1 \times 1^2, 2048$	$1 \times 1 \times 1$
fc_2		$1 \times 1^2, \#\text{classes}$	$1 \times 1 \times 1$

Table 4: **X3D-M model architecture.** When converted to a continual CNN, the highlighted components carry an internal state which results in a memory overhead. *Temporal kernel size in conv_1 is set to 5 as found in the official X3D source code www.github.com/facebookresearch/SlowFast.

B. Benchmarking details

This section should be read in conjunction with Section 4.4 of the main paper. To gauge the achievable on-hardware speeds of clip and frame predictions, a benchmark was performed on the following four system: A CPU core of a MacBook Pro (16-inch 2019 2.6 GHz Intel Core i7); Nvidia Jetson TX2; Nvidia Jetson Xavier; and a Nvidia RTX 2080 Ti GPU (on server with Intel XEON Gold processors). A batch size of 1 was used for testing on CPU, while the largest fitting multiple of 2^N up to 64 was used for the other hardware platforms which have GPUs and lend themselves better to parallelisation. Thus, the speeds noted for GPU platforms in Table 1 of the main paper should not be interpreted as the number of processed clips/frames from a single (high-speed) video stream, but rather as the aggregated number of clips/frames from multiple streams using the available hardware. The exact batch size and input resolutions can be found in Table 5. In conducting the measurements, we assume the input data is readily available on the CPU and measure the time it takes for it to transfer from the CPU to GPU (if applicable), process, and transfer back to the CPU. A precision of 16 bits was used for the embedded platforms TX2 and Xavier, while a 32 bit precision was employed for CPU and RTX 2080 Ti. All networks were implemented and tested using PyTorch, and neither Nvidia TensorRT nor ONNX Runtime were used to speed up inference.

Model	Input shape ($T \times S^2$)	Batch size			
		CPU	TX2	Xavier	RTX
I3D-R50	8×224^2	1	16	16	32
R(2+1)D-18 ₈	8×112^2	1	16	16	32
R(2+1)D-18 ₁₆	16×112^2	1	8	16	32
SlowFast-8x8-R50	8×256^2	1	8	32	32
SlowFast-4x16-R50	16×256^2	1	16	32	32
X3D-L	16×312^2	1	16	32	32
X3D-M	16×224^2	1	32	64	64
X3D-S	13×160^2	1	64	64	64
X3D-XS	4×160^2	1	64	64	64
CoX3D-L	1×312^2	1	8	16	32
CoX3D-M	1×224^2	1	32	64	64
CoX3D-S	1×160^2	1	32	64	64

Table 5: **Benchmark model configurations.** For each model, the input shape is noted as $T \times S^2$, where T and S are the temporal and spatial input shape.